Retinotopic specializations of cortical and thalamic inputs to area MT

Inaki-Carril Mundinano[a], William C. Kwan[a], and James A. Bourne[a,1]

[a]Australian Regenerative Medicine Institute, Monash University, Clayton, VIC 3800, Australia

Edited by Tony Movshon, New York University, New York, NY, and approved October 10, 2019 (received for review June 6, 2019)

Retinotopic specializations in the ventral visual stream, especially foveal adaptations, provide primates with high-acuity vision in the central visual field. However, visual field specializations have not been studied in the dorsal visual stream, dedicated to processing visual motion and visually guided behaviors. To investigate this, we injected retrograde neuronal tracers occupying the whole visuotopic representation of the middle temporal (MT) visual area in marmoset monkeys and studied the distribution and morphology of the afferent primary visual cortex (V1) projections. Contrary to previous reports, we found a heterogeneous population of V1-MT projecting neurons distributed in layers 3C and 6. In layer 3C, spiny stellate neurons were distributed mainly in foveal representations, while pyramidal morphologies were characteristic of peripheral eccentricities. This primate adaptation of the V1 to MT pathway is arranged in a way that we had not previously understood, with abundant stellate projection neurons in the high-resolution foveal portions, suggesting rapid relay of motion information to visual area MT. We also describe that the medial portion of the inferior pulvinar (PIm), which is the main thalamic input to area MT, shows a retinotopic organization, likely reflecting the importance of this pathway during development and the establishment of area MT topography.

nonhuman primate | spiny stellate neurons | pulvinar | retinotopy | primary visual cortex

The visual system of primates comprises multiple interconnected cortical and thalamic areas. Neurons in a subset of areas are arranged into visual maps, derived from the retina and enforced through topographically organized cortical (1, 2) and thalamic (3) connections. This can be expressed as a strict first-order mapping of the visual field across the brain tissue, as observed in the lateral geniculate nucleus (LGN), primary visual cortex (V1), and middle temporal visual area (MT or V5), or a fragmented mapping with discontinuities, as observed in many extrastriate areas (4).

Visual area MT, a small extrastriate cortical area that processes visual motion, has been the subject of numerous anatomic and physiological investigations, as it is central to the functional organization of primate cerebral cortex. The evolution of area MT seems to be unique to the primate lineage (5); its early development, connectivity, and critical role in dorsal stream maturation indicate that MT is a primary-like area (6–8). In the adult, the main inputs to area MT arrive from the primary visual cortex (V1) (9). In early development, area MT receives strong input from the medial subdivision of the inferior pulvinar (PIm) in the thalamus, which is the recipient of retinal input (10, 11). While the visual topography of connections between V1 and MT is well established (12–14), the topography of the thalamocortical projection from PIm has not been determined. Thus, if the primary-like area theory for area MT is correct, then area PIm would be expected to present a first-order visual topography.

To investigate whether a first-order representation of the visual field is present in the PIm, we performed multiple injections of neural tracers in area MT of the marmoset monkey (*Callithrix jacchus*), covering the entire representation of the contralateral visual field (Fig. 1 *A*, *B*, and *B′*). Subsequently, we analyzed the input from the PIm to determine whether neurons there were arranged in a visuotopic manner (Fig. 1*C* and *SI Appendix*, Fig. S1). In parallel, we were able to study in detail the anatomy of the V1-MT connection stemming from the same injections in MT. In the macaque, the main input to MT originates from layer 3C of V1 and is organized by partially segregated pathways originating from cells with different morphology: spiny stellate neurons, which carry mainly magnocellular (motion) information, and pyramidal neurons relaying more complex magnocellular, parvocellular, and koniocellular inputs to MT (15). In New World monkeys, including the common marmoset, the anatomic specialization of this projection has been controversial, since previous authors did not find spiny stellate neurons in the corresponding layer of V1 (13, 16, 17). The suggestion that this population of cells is absent from the New World monkeys is at odds with much of our understanding of the evolution of the visual cortex, especially the theory that both V1 and MT have "anchored" the evolution of the primate visual cortex (4). To address the critical nature of area MT in the primate visual cortex, we studied the neuroanatomy and morphology of the MT-projecting V1 neurons in relation to their visual topography, mapped the retinotopic organization of the PIm-MT connection, and evaluated their functional implications.

Results

Area MT Is the Recipient of a First-Order Retinotopic Input from the Medial Subdivision of the PI. Stereotaxic injections of anterograde and retrograde neural tracers into specific retinotopic regions of area MT (*SI Appendix*, *SI Methods*) revealed a first-order visuotopic organization in the PIm. The retinotopic map of the PIm contained upper and lower visual field representations. The horizontal meridian (HM) was represented obliquely, dividing the PIm in 2 (Fig. 1*D*). In the most caudal third of the PIm, the upper visual

Significance

Foveal specializations in the primate visual system have allowed for high-acuity vision and are crucial to the evolution of the brain and primate behaviors. Here we show that the dorsal visual stream, which is dedicated to processing visual motion and visually guided behaviors, comprises foveal specializations. We report that spiny stellate cells, an anatomically specialized type of projection neuron, are distributed mainly in the foveal portion of the primary visual cortex (V1)-middle temporal area (MT) pathway. Moreover, we demonstrate that the thalamic input to the MT area from the medial inferior pulvinar is organized in a retinotopic manner. These results change our understanding of the anatomic organization of the early visual system.

Author contributions: I.-C.M. and J.A.B. designed research; I.-C.M., W.C.K., and J.A.B. performed research; I.-C.M., W.C.K., and J.A.B. analyzed data; and I.-C.M. and J.A.B. wrote the paper.

The authors declare no competing interest.

This article is a PNAS Direct Submission.

[1]To whom correspondence may be addressed. Email: james.bourne@monash.edu.

This article contains supporting information online at www.pnas.org/lookup/suppl/doi:10.1073/pnas.1909799116/-/DCSupplemental.

First published October 28, 2019.

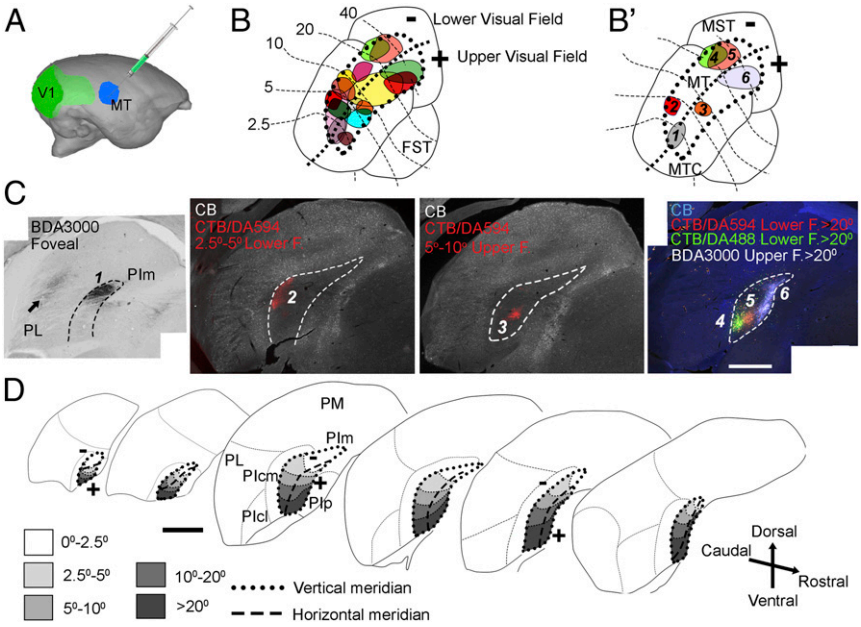

Fig. 1. Multiple MT tracer injections revealed a topographic organization of the PIm. (*A*) 3D reconstruction of a marmoset brain highlighting area MT and V1. (*B*) Graphic representation of all the injection sites in area MT. Each color represents one injection. Details are provided in *SI Appendix*, Table S1. (*B′*) Representative examples of MT injections at different eccentricities in the upper and lower visual field representations. (*C*) Photomicrographs of pulvinar sections showing retrograde labeled cells in PIm. Numbers indicate the corresponding injection sites in *B′*. Dashed lines indicate the borders of the PIm, delineated by calbindin (CB) immunohistochemistry. The arrow indicates the band of anterograde labeling in the foveal representation of the lateral pulvinar. (*D*) Proposed visuotopic organization of Pim. (Scale bars in *C* and *D*: 1 mm.)

field had a broader representation and was located ventromedially. In the middle third of the subdivision, the HM divided the PIm into 2 halves, with the upper field located medial to the HM. The rostral portion of the PIm was largely occupied by the lower visual field in the lateral part of the structure.

The representation of the vertical meridian (VM) was located on the boundaries of the PIm, juxtaposing adjacent PIm subdivisions (PIcm and PIp). PIm neurons projecting to foveal representations of area MT were located in the most dorsal portion of the PIm, while neurons connecting to peripheral eccentricities were located ventrally (Fig. 1*D*). In our estimated PIm visuotopic map, and similarly to the lateral geniculate nucleus (3), foveal and parafoveal eccentricities (0 to 5 degrees) occupied 36% of the area, while 70% of the PIm area was devoted to the first 20 degrees of eccentricity.

Interestingly, in addition to the well-established connection with the PIm, we found a foveal specialized connection between MT and the lateral subdivision of the pulvinar (PL). Tracer injections in the foveal representation of area MT revealed a band of mostly anterograde labeling in PL that was not observed following injections in other eccentricities (Fig. 1*C*). This MT-PL connection corresponded to the foveal topography previously described in the primate PL (18–20).

All retrogradely labeled cells in the PIm expressed the glutamatergic marker glutaminase (Fig. 2*A*) and were weakly immunopositive for the calcium-binding protein parvalbumin (PV) (Fig. 2 *B* and *C*). In PIm, 2 populations of PV^+ neurons were present: those that weakly stain for PV, which have been suggested to be projection neurons associated with "driver"-type thalamocortical inputs (21, 22), and those that highly express PV, morphologically similar to interneurons (*SI Appendix*, Fig. S2). Here we confirm the glutamatergic phenotype of the PIm-MT relay. Interestingly, all retrograde-labeled PIm-MT projecting neurons were immunopositive for Ca^{2+}/calmodulin-activated protein kinase II alpha (CamKIIα) (Fig. 2*D*). CamKIIα expression was restricted to PIm, showing no positive immunoreactivity in PIp or PIcm (Fig. 2*E*), suggesting a different function for the different PIm subunits.

LGN-MT Neurons Are a Small Population. In agreement with previous descriptions in the marmoset, we found a small population of neurons in the koniocellular layers of the LGN projecting to area MT (7). In fact, LGN-MT neurons were 0.8 ± 0.5% of the total retrograde labeled cells; PIm-MT neurons were 23.4% ±8.6, while V1-MT neurons were 75.8% ± 8.5 (n = 14 injections, 10,344 total neurons; 7 animals) (*SI Appendix*, Fig. S3). Similar to the macaque, LGN-MT neurons were immunopositive for CamKIIα (23) (*SI Appendix*, Fig. S2*B*) and had a retinotopic organization as described previously (3).

V1-MT Projecting Neurons Are a Heterogeneous Population. Retrograde neuronal tracer injections in area MT revealed that there were different morphological populations of labeled neurons in V1. Cells were principally located in layer 3C (82%), layer 6 (15%), and layer 5 (3%) (Fig. 3*A*).

In layer 3C, 4 morphologically different populations of neurons were identified; large pyramidal neurons, small pyramidal neurons, large spiny stellate neurons, and small spiny stellate neurons (15%, 59%, 8%, and 18%, respectively of the total labeled neurons in layer 3C; n = 10,919 neurons, 16 injections, and 8 animals) (Fig. 3*B*). Pyramidal neurons, both large and small, could be discerned by the presence of an apical dendrite extending perpendicularly toward the surface of the cortex and a cluster of basal spiny dendrites. Large pyramidal neurons had a triangular soma (>160 μm^2; 223 ± 50 μm^2), while the small pyramidal neuron soma (<160 μm^2; 105 ± 31) was normally more rounded (Fig. 3 *B*, *Top*). For both large and small spiny stellates, the dendritic arbor projected radially around the soma and was mostly confined within the limits of layer 3C. Large stellate neurons were located in the most ventral portion of layer 3C, with some of their dendritic ramifications extending into the magnocellular recipient layer 4A (Fig. 3 *B*, *Bottom Left*). Large (231 ± 62 μm^2)

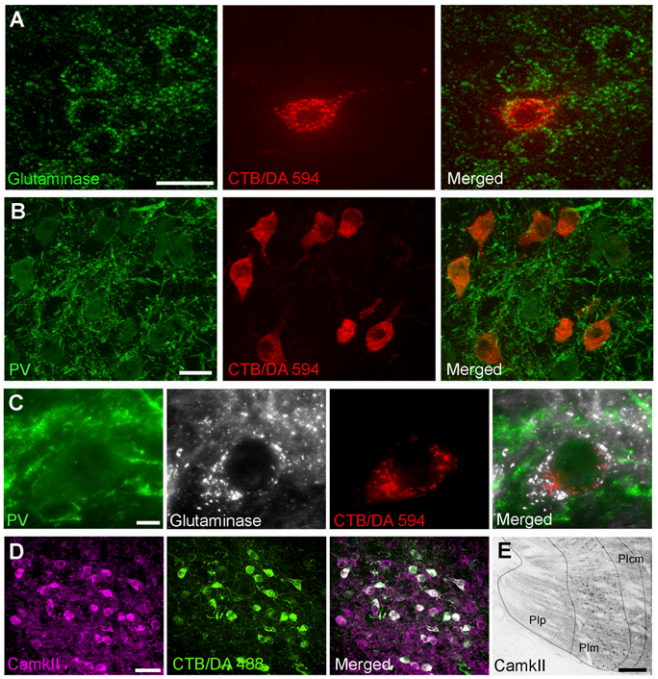

Fig. 2. Immunochemical characterization of PIm-MT projecting neurons. (*A*) Photomicrographs showing a retrograde labeled neuron expressing the glutamatergic marker glutaminase. (*B*) PIm-MT neurons immunoreactive for PV. (*C*) Colocalization of glutaminase and PV in retrogradely labeled PIm neurons. (*D*) Retrogradely labeled PIm neurons immunopositive for CamKIIα. (*E*) Low-power micrograph showing CamKIIα expression restricted to the Pim and absent in the adjacent subnuclei (Scale bars: 20 μm in *A*, *B*, and *E*; 5 μm in *C*; 50 μm in *D*).

and small (109 ± 32 μm^2) stellates were distinguishable by soma larger and smaller than 160 μm^2, respectively (Fig. 3*C*). Sholl analysis performed to quantify the morphological characteristics of the 4 populations of cells revealed that spiny stellate neurons had a significantly more complex basal dendritic organization compared with pyramidal neurons (Fig. 3*D*), allowing the 2 populations of cells to be distinguished. However, there was no significant difference in dendritic organization between large and small cells of the same phenotype (*SI Appendix*, Fig. S4).

The percentages of the different populations of neurons in layer 3C varied depending on their location within the retinotopic representation of the visual field (Fig. 3 *E* and *F*). In operculum V1, where foveal and parafoveal eccentricities of the visual field (between 0° and 5°) are represented, we observed the highest numbers of spiny stellate neurons (36.1% small stellates and 16.3% large stellates) (Fig. 3*E*). Within the operculum, the number of spiny stellate neurons decreased following a lateromedial gradient (Fig. 3*F*), revealing that a greater number of stellates are associated with more foveal representations, while along the medial surface of V1 and through the calcarine sulcus, the majority of neurons had a pyramidal morphology. Interestingly, spiny stellate neurons in these areas were concentrated around the horizontal meridian representation, in the fundus of the calcarine sulcus (Fig. 3*C*). The number of pyramidal neurons increased following an anteroposterior increasing gradient.

In regions of V1 where eccentricity was below the first 20 degrees, cells within layer 3C were grouped forming clusters of the same morphology (Fig. 3 *B*, *Top Left*). Previous studies in the macaque monkey (24) showed that MT-projecting pyramidal neuron clusters were located preferentially underneath the layer 2/3 cytochrome oxidase (CO)-positive blobs and MT-projecting stellate cells underneath the interblob space. Our results, although in general agreement with this description, are not sufficiently conclusive to affirm that all pyramids are beneath the CO blobs (*SI Appendix*, Fig. S5). For example, in the rostral parts of calcarine V1 (>20 degrees of eccentricity), where most of the neurons were pyramidal, these cells clusters were not apparent, and V1-MT projecting neurons were more evenly distributed.

The second most abundant population of V1-MT projecting neurons were localized in layer 6 and characterized as Meynert cells (25) (*SI Appendix*, Fig. S6). The soma of Meynert cells (396 ± 171 μm^2) were significantly larger than those of all V1-MT projecting cells in layer 3C [$F(4, 2{,}366) = 389.8$; $P < 0.0001$; ANOVA]. Previous studies in the macaque have described layer 6 Meynert cells as nontufted pyramids with broad cell bodies and lateral dendrites extending for long distances (26). Our findings in the marmoset coincide with the morphological description for the macaque, although depending on the area of V1, we could detect some morphological variations. For example, along the medial surfaces of calcarine V1, some Meynert cells had a thick apical dendrite with an enlarged proximal section of the apical dendrite at the junction with the soma and an elongated cell body (*SI Appendix*, Fig. S6*B*). Meanwhile, in operculum V1, we could not find any Meynert cell with this morphology. Some Meynert cells in the operculum had a thin apical dendrite with no thickened proximal section. Other cells had smaller soma with no apparent apical dendrite. The percentage of Meynert cells observed with traditional tracers (BDA and CTB/DA) was 6% of the total number of cells ($n = 7{,}863$); however, the viral tracer AAV-retro-hSyn-EGFP revealed a significantly higher proportion of Meynert cells (15%). In this case, Meynert cells were more abundant in the calcarine sulcus and medial surface of V1 (23%) than in the operculum (11%).

Only the viral tracer injections revealed a population of neurons located in lower layer 5, where they composed 3% of the total number of V1-MT projecting cells and were homogenously distributed within V1, revealing no changes with eccentricity. These cells were all of a pyramidal morphology with an intermediate soma size (167 ± 35 μm^2) (*SI Appendix*, Fig. S6*A*). Similarly, in the macaque, Nahn and Callaway (25) found a single cell in layer 5 of V1 after injection of G-deleted rabies virus in area MT.

Discussion

The PIm-MT Connection Is Retinotopically Organized and Glutamatergic. The past few years have brought a re-emergence of interest in the visual pulvinar nuclei (lateral and inferior), in terms of its connectivity and role in visual processing (27, 28). This has originated in part because of the possibility of linking specific circuits to behaviors and their association with the establishment of visual cortical areas and associated processing networks, such as the dorsal and ventral streams (29, 30), and the potential involvement in "blindsight" (27). The PL is connected to V1 and other extrastriate areas of the ventral stream, while the PIm is the primary thalamic input to area MT, a major component of the dorsal stream (11, 30). Previous electrophysiological neural tracing studies in New World (18, 31) and Old World monkeys (19) and functional MRI studies in humans (32) have demonstrated a visuotopic organization of the PL and the inferior centrolateral subdivision (PIcl). However, only a gross description of the horizontal and vertical meridians has been provided for PIm (33), with the suggestion that it is likely to have a discontinuous, second-order representation of the visual field. Here we describe a complete visual field retinotopic organization of the PIm-MT pathway that is more akin to the first-order LGN-V1 relay.

An ongoing confounder regarding the PIm has been the origin of the visual input. While there was early evidence of retinal input (10, 34) and demonstration of the plasticity of this retinopulvinar pathway during the early postnatal period (7), it has been consistently suggested that the main input originates from the superior colliculus (SC) (35, 36). However, most recently we

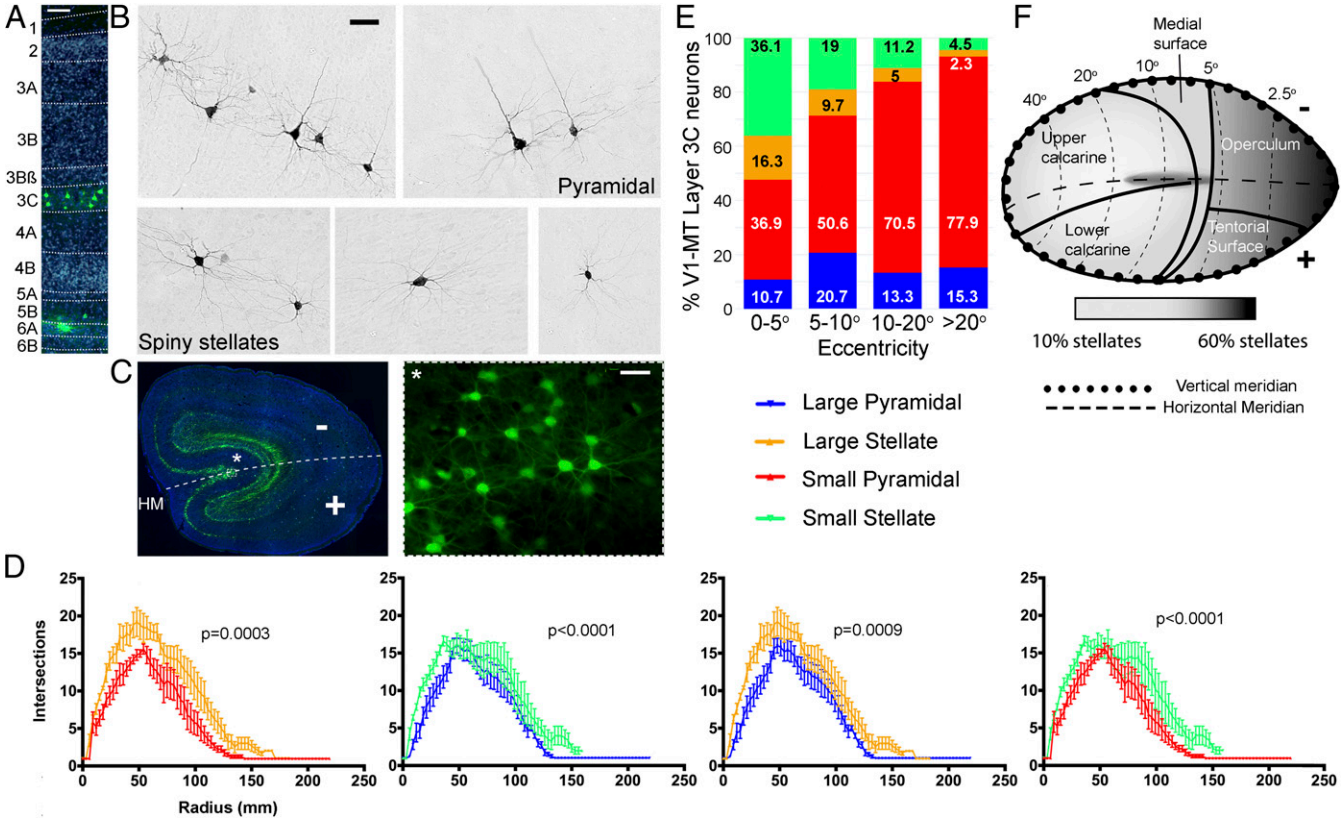

Fig. 3. Morphology of V1-MT projecting neurons depends on eccentricity. (*A*) Photomicrograph of V1 showing the cortical layers. Note the retrograde labeled cells in layers 3C, 5B, and 6A. (*B*) Images of retrograde cells in V1 layer 3C with different morphologies. (*Top Left*) Image showing 2 clusters of spiny stellates (*Left*) and pyramidal neurons (*Right*). (*Top Right*) Image showing 2 pyramidal neurons, large and small. (*Bottom*) Images showing different small and large spiny stellate cells. (*C*) Image of a caudal coronal section of area V1 with retrograde labeled neurons following injection in area MT. (*Inset*) Spiny stellate cells in the representation of the HM, area denoted by *. (*D*) Sholl analysis graphs showing significant differences in the organization of the basal dendritic arbors among pyramidal and spiny stellate neurons. (*E*) Chart showing percentages of different layer 3C V1-MT projecting neuronal morphologies at different eccentricities of the visual field. (*F*) Flat map representation of area V1. The gray gradient represents the percentage of stellate neurons in layer 3C. [Scale bars: 100 μm in *A*; 1 mm in *C*; 50 μm in *B* and *C* (*Inset*).]

have been able to clearly demonstrate using more robust neural tracing techniques that the PIm receives retinal but not SC connections, and furthermore, that these retinal inputs are not collaterals of projections to the LGN or SC (11). In contrast, the flanking posterior (PIp), centromedial (PIcm), and PIcl subdivisions of the PIm receive both SC and LGN inputs (11). Furthermore, we have also previously demonstrated that this early PIm relay of retinal information is crucial for the maturation of MT (6, 7, 37) and establishment of behaviors linked to the dorsal visual stream (8). These observations led to the hypothesis that area MT might act as a primary-like cortical area, and that the retinopulvinar-MT pathway drives the visual sensory experience-dependent maturation of the dorsal stream (6, 8). Therefore, the evidence that we provide here of a first-order topographic representation of the visual field in PIm further supports the hypothesis that area MT is a primary-like constituent of the dorsal stream.

Accordingly, we have shown that all PIm-MT projecting neurons are glutamatergic and parvalbumin immunopositive, which is in agreement within the core-matrix theory of thalamocortical connectivity, where PV^+ neurons provide driver input to the cortex from the primary relay nucleus with a strict topographical organization (21, 22). In addition, and similar to the LGN-MT projecting neurons, we found that all of the PIm-MT neurons also express CamKIIα. The NMDA receptor-CamKIIα complex is critical to the induction of long-term potentiation (38), a mechanism proposed to underlie sensory experience-dependent strengthening and plasticity of thalamocortical synapses during early development (39, 40). This result is in line with our recent study demonstrating that early-life PIm-MT input is crucial for the correct development and maturation of area MT (8). Furthermore, it can be suggested that the PIm-MT relay is responsible for establishing the first-order topographic map in area MT, which is observed before the arrival of V1-MT neurons (7).

Further evidence in support of this hypothesis comes from electrophysiological studies of MT following early-life lesions of V1 (41). Subsequent to the lesion, the retinotopic organization of area MT remains intact in the lesion projection zone into adulthood, although they show alterations in direction selectivity. Thus, we suggest that the developmental mechanisms leading to initial formation of the retinotopic organization of area MT are dependent on the relay originating in the PIm, while tuning of neurons for direction selectivity relies on inputs from V1.

While the LGN is also organized in a first-order manner and the K-layers project to area MT, only a few cells are observed following the MT injections, with many orders of numbers lower than those originating from the PIm. The reduced numbers of LGN-MT neurons compared with PIm-MT neurons might have implications supporting a major role of the retinopulvinar-MT pathway as the neural substrate for residual vision phenomena after V1 lesions, especially in early life (27, 42, 43). Furthermore, the scarcity across the full retinotopy of the LGN suggests that

they are less likely to have been responsible for the establishment of the topographic map in area MT.

Foveal V1-MT Neurons Show Anatomic Specialization in Layer 3C. Foveal vision in primates is highly specialized throughout the whole visual system, originating in the cellular and vascular adaptations of the central retina (44) and extending to the expansion of the geniculate parvocellular pathway (45) and the high neuronal density of the geniculorecipient layers of the V1 cortex. These adaptations have allowed for high-acuity central vision (46) and trichromacy (47), shaping much of the primate behavior through evolution of the ventral visual pathway (48). Here we show that foveal specialization also characterizes the magnocellular dorsal visual pathway, demonstrating that foveal portions of the V1-MT pathway are populated with abundant spiny stellate projection neurons, while more peripheral eccentricities projection neurons are mostly of pyramidal morphology.

The functional relevance of the morphologically segregated neuronal populations in relation to the visual field can be explained from different perspectives. In primates, layer 3C of V1, where most of the MT projection neurons are located, spiny stellate neurons receive almost exclusive magnocellular input from cells in layer 4A (15, 24, 49), and those underneath the CO interblob regions are generally tuned for a specific orientation. Furthermore, stellate neurons show higher sensitivity to small inputs, and their firing rates are also higher (50). Thus, high numbers of foveal stellate neurons might be necessary to mediate faster and more precise information to motion processing area MT than to other channels. On the other hand, given their preferential position under the CO blobs, layer 3C pyramidal neurons can receive parvocellular and koniocellular input through the apical dendrite branches in layers 2/3 and 1 and can send more complex visual motion information to area MT.

The decreasing gradient with the eccentricity of the stellate vs. pyramid ratio also might contribute to the observed differences in the electrophysiological properties of foveal and peripheral V1. The smaller receptive fields (2), larger point image sizes (51), and slower spatiotemporal interactions (52) of foveal V1 neurons compared with peripheral V1 neurons also might be influenced by the functional properties of spiny stellate neurons. Interestingly, this proposed mechanism might also be occurring in regions of V1 representing the horizontal meridian (fundus of the calcarine sulcus), where we detected a majority of stellate neurons (Fig. 3 *C* and *F*). This potentially has implications for the oblique effect observed in humans and research animals, where sensitivity to orientation and visual performance are enhanced for cardinal stimuli, especially along the horizontal meridian, where the stellate population was highest (53). Accordingly, the oblique effect is represented in area MT as a larger proportion of its area devoted to the cardinal orientations (54).

Previous reports describing layer 3C V1 neurons projecting to area MT in the marmoset monkey suggested that they were mostly or entirely of pyramidal morphology (13, 16, 17). This has been considered one of the major differences between macaque and marmoset visual systems, and the absence of stellate cells reflects a limitation in the species processing capability. Results from this study, however, categorically demonstrates V1-MT neurons in the marmoset form a heterogeneous population similar to that described for the macaque (25, 49, 55) and the New World squirrel monkey (56). One simple explanation for the discrepancies with previous studies in marmosets is that the distribution of spiny stellate neurons correlates with foveal and parafoveal eccentricities, with the largest concentration seen in the foveal representation of the operculum. Previously, vogt Weisenhorn et al. (16) described MT projecting neurons only in calcarine V1, where the spiny stellate neurons are not abundant. On the other hand, Elston and Rosa (17) reported a small population of spiny stellate neurons in layer 3C, but they did not analyze this further. The morphology of V1-MT neurons in the macaque has been traditionally qualified as mainly spiny stellate; however, pyramidal neurons at different proportions have been described as well (25, 55, 57). In these studies, the most abundant percentages of pyramidal neurons were located in V1 regions with peripheral eccentricities. For example, Shipp and Zeki (57) found 20% of V1 pyramidal cells following their central MT injections, but this percentage doubled to 40% with their most peripheral MT injection. Moreover, in the same study, the authors affirmed that in 3 owl monkeys, which, interestingly, do not have a fovea (58), area MT projecting V1 neurons were purely pyramidal, where their injections occupied 5 to 90 degrees of eccentricity. More recently, Nanh and Callaway (25) characterized the same neuronal populations in the macaque as 82% spiny stellate and 18% pyramids, but to our knowledge they did not provide details or consider the retinotopy of V1. In agreement with our results in the marmoset, in the macaque, Elston and Rosa (55) found 68% pyramids and 31% stellates when MT tracer deposits occupied the visuotopic region of 5 to 30 degrees of eccentricity. Thus, our results unambiguously confirm that in the marmoset, the spiny stellate cell population in layer 3C is preferentially located in the foveal and parafoveal representations, while pyramidal neurons are more abundant in peripheral V1 regions.

The visual system of Old World and New World monkeys, although presenting some obvious differences, particularly relating to brain size, are very similar in organization and function. In both Old World and New World monkeys, the V1-MT pathway carries direct magnocellular visual input, crucial for dorsal stream-associated behaviors such as motion detection and visually-guided behaviors. Mitchell and Leopold (59) have provided a detailed comparison of the marmoset and macaque visual systems. The foveal specialization of the V1-MT pathway described here is conserved in Old World monkeys and might be important for more efficient processing of the central and cardinal visual field inputs for dorsal stream-related behaviors. Taken together with the evidence outlined above, our findings suggest that this cellular organization is conserved across primates. This is crucial information and provides further evidence indicating the close similarity in the visual systems of marmosets and Old World species and suggesting that the origin of this specialization is further back in evolution than originally predicted.

Materials and Methods

A total of 8 New World marmoset (*C. jacchus*) monkeys were used in this study. All experiments were conducted in accordance with the Australian Code of Practice for the Care and Use of Animals for Scientific Purposes and were approved by the Monash University Animal Ethics Committee, which also monitored the welfare of the animals. To map the complete topography and cellular morphology of the primary thalamocortical and cortico-cortical visual inputs to area MT, different neuronal tracers were pressure-injected to occupy the whole volume of area MT. Retrogradely labeled cells in V1 were qualified and compared by Sholl analysis. Retrograde labeling in PIm was analyzed to reveal the retinotopic organization of the connection. Retrogradely labeled cells in PIm and LGN were immunohistochemically analyzed. More details are provided in *SI Appendix*.

ACKNOWLEDGMENTS. We thank Dr. David A. Leopold and Dylan M. Fox for their helpful advice interpreting the results and Dr. Gang Zheng (Monash Biomedical Imaging) for his assistance with MRI acquisition. This work was supported by an Australian National Health and Medical Research Council (NHMRC) Project Grant (APP1138038). J.A.B. is supported by an NHMRC Senior Research Fellowship (APP1077677). The Australian Regenerative Medicine Institute is supported by grants from the State Government of Victoria and the Australian Government.

1. D. C. Van Essen, W. T. Newsome, J. H. Maunsell, The visual field representation in striate cortex of the macaque monkey: Asymmetries, anisotropies, and individual variability. *Vision Res.* **24**, 429–448 (1984).
2. K. A. Fritsches, M. G. P. Rosa, Visuotopic organisation of striate cortex in the marmoset monkey (Callithrix jacchus). *J. Comp. Neurol.* **372**, 264–282 (1996).
3. A. J. R. White, H. D. Wilder, A. K. Goodchild, A. J. Sefton, P. R. Martin, Segregation of receptive field properties in the lateral geniculate nucleus of a New-World monkey, the marmoset Callithrix jacchus. *J. Neurophysiol.* **80**, 2063–2076 (1998).
4. M. G. Rosa, Visual maps in the adult primate cerebral cortex: Some implications for brain development and evolution. *Braz. J. Med. Biol. Res.* **35**, 1485–1498 (2002).
5. L. Krubitzer, D. M. Kahn, Nature versus nurture revisited: An old idea with a new twist. *Prog. Neurobiol.* **70**, 33–52 (2003).
6. I. C. Mundinano, W. C. Kwan, J. A. Bourne, Mapping the mosaic sequence of primate visual cortical development. *Front. Neuroanat.* **9**, 132 (2015).
7. C. E. Warner, W. C. Kwan, J. A. Bourne, The early maturation of visual cortical area MT is dependent on input from the retinorecipient medial portion of the inferior pulvinar. *J. Neurosci.* **32**, 17073–17085 (2012).
8. I.-C. Mundinano *et al.*, Transient visual pathway critical for normal development of primate grasping behavior. *Proc. Natl. Acad. Sci. U.S.A.* **115**, 1364–1369 (2018).
9. L. A. Krubitzer, J. H. Kaas, Cortical connections of MT in four species of primates: Areal, modular, and retinotopic patterns. *Vis. Neurosci.* **5**, 165–204 (1990).
10. C. E. Warner, Y. Goldshmit, J. A. Bourne, Retinal afferents synapse with relay cells targeting the middle temporal area in the pulvinar and lateral geniculate nuclei. *Front. Neuroanat.* **4**, 8 (2010).
11. W. C. Kwan *et al.*, Unravelling the subcortical and retinal circuitry of the primate inferior pulvinar. *J. Comp. Neurol.* **527**, 558–576 (2019).
12. M. G. Rosa, G. N. Elston, Visuotopic organisation and neuronal response selectivity for direction of motion in visual areas of the caudal temporal lobe of the marmoset monkey (Callithrix jacchus): Middle temporal area, middle temporal crescent, and surrounding cortex. *J. Comp. Neurol.* **393**, 505–527 (1998).
13. W. B. Spatz, Topographically organized reciprocal connections between areas 17 and MT (visual area of superior temporal sulcus) in the marmoset Callithrix jacchus. *Exp. Brain Res.* **27**, 559–572 (1977).
14. S. M. Palmer, M. G. Rosa, A distinct anatomical network of cortical areas for analysis of motion in far peripheral vision. *Eur. J. Neurosci.* **24**, 2389–2405 (2006).
15. J. J. Nassi, E. M. Callaway, Parallel processing strategies of the primate visual system. *Nat. Rev. Neurosci.* **10**, 360–372 (2009).
16. D. M. vogt Weisenhorn, R. B. Illing, W. B. Spatz, Morphology and connections of neurons in area 17 projecting to the extrastriate areas MT and 19DM and to the superior colliculus in the monkey Callithrix jacchus. *J. Comp. Neurol.* **362**, 233–255 (1995).
17. G. N. Elston, M. G. Rosa, Ipsilateral corticocortical projections to the primary and middle temporal visual areas of the primate cerebral cortex: Area-specific variations in the morphology of connectionally identified pyramidal cells. *Eur. J. Neurosci.* **23**, 3337–3345 (2006).
18. J. M. Allman, J. H. Kaas, R. H. Lane, F. M. Miezin, A representation of the visual field in the inferior nucleus of the pulvinar in the owl monkey (Aotus trivirgatus). *Brain Res.* **40**, 291–302 (1972).
19. D. B. Bender, Retinotopic organization of macaque pulvinar. *J. Neurophysiol.* **46**, 672–693 (1981).
20. L. G. Ungerleider, T. W. Galkin, R. Desimone, R. Gattass, Subcortical projections of area V2 in the macaque. *J. Cogn. Neurosci.* **26**, 1220–1233 (2014).
21. E. G. Jones, S. H. C. Hendry, Differential calcium binding protein immunoreactivity distinguishes classes of relay neurons in monkey thalamic nuclei. *Eur. J. Neurosci.* **1**, 222–246 (1989).
22. R. W. Guillery, S. M. Sherman, Thalamic relay functions and their role in corticocortical communication: Generalizations from the visual system. *Neuron* **33**, 163–175 (2002).
23. L. C. Sincich, K. F. Park, M. J. Wohlgemuth, J. C. Horton, Bypassing V1: A direct geniculate input to area MT. *Nat. Neurosci.* **7**, 1123–1128 (2004).
24. J. J. Nassi, E. M. Callaway, Specialized circuits from primary visual cortex to V2 and area MT. *Neuron* **55**, 799–808 (2007).
25. H. L. Nhan, E. M. Callaway, Morphology of superior colliculus- and middle temporal area-projecting neurons in primate primary visual cortex. *J. Comp. Neurol.* **520**, 52–80 (2012).
26. W. E. le Gros Clark, The cells of Meynert in the visual cortex of the monkey. *J. Anat.* **76**, 369–376.1 (1942).
27. H. Bridge, D. A. Leopold, J. A. Bourne, Adaptive pulvinar circuitry supports visual cognition. *Trends Cogn. Sci.* **20**, 146–157 (2016).
28. G. Purushothaman, R. Marion, K. Li, V. A. Casagrande, Gating and control of primary visual cortex by pulvinar. *Nat. Neurosci.* **15**, 905–912 (2012).
29. M. A. Goodale, A. D. Milner, Separate visual pathways for perception and action. *Trends Neurosci.* **15**, 20–25 (1992).
30. J. H. Kaas, D. C. Lyon, Pulvinar contributions to the dorsal and ventral streams of visual processing in primates. *Brain Res. Brain Res. Rev.* **55**, 285–296 (2007).
31. R. Gattass, E. Oswaldo-Cruz, A. P. Sousa, Visuotopic organization of the cebus pulvinar: A double representation the contralateral hemifield. *Brain Res.* **152**, 1–16 (1978).
32. M. J. Arcaro, M. A. Pinsk, S. Kastner, The anatomical and functional organization of the human visual pulvinar. *J. Neurosci.* **35**, 9848–9871 (2015).
33. A. Dick, A. Kaske, O. D. Creutzfeldt, Topographical and topological organization of the thalamocortical projection to the striate and prestriate cortex in the marmoset (Callithrix jacchus). *Exp. Brain Res.* **84**, 233–253 (1991).
34. B. J. O'Brien, P. L. Abel, J. F. Olavarria, The retinal input to calbindin-D28k-defined subdivisions in macaque inferior pulvinar. *Neurosci. Lett.* **312**, 145–148 (2001).
35. R. A. Berman, R. H. Wurtz, Signals conveyed in the pulvinar pathway from superior colliculus to cortical area MT. *J. Neurosci.* **31**, 373–384 (2011).
36. D. C. Lyon, J. J. Nassi, E. M. Callaway, A disynaptic relay from superior colliculus to dorsal stream visual cortex in macaque monkey. *Neuron* **65**, 270–279 (2010).
37. J. A. Bourne, M. G. Rosa, Hierarchical development of the primate visual cortex, as revealed by neurofilament immunoreactivity: Early maturation of the middle temporal area (MT). *Cereb. Cortex* **16**, 405–414 (2006).
38. J. Lisman, R. Yasuda, S. Raghavachari, Mechanisms of CaMKII action in long-term potentiation. *Nat. Rev. Neurosci.* **13**, 169–182 (2012).
39. D. E. Feldman, Synaptic mechanisms for plasticity in neocortex. *Annu. Rev. Neurosci.* **32**, 33–55 (2009).
40. A. Kirkwood, M. C. Rioult, M. F. Bear, Experience-dependent modification of synaptic plasticity in visual cortex. *Nature* **381**, 526–528 (1996).
41. H. H. Yu *et al.*, Visually evoked responses in extrastriate area MT after lesions of striate cortex in early life. *J. Neurosci.* **33**, 12479–12489 (2013).
42. C. E. Warner *et al.*, Preservation of vision by the pulvinar following early-life primary visual cortex lesions. *Curr. Biol.* **25**, 424–434 (2015).
43. I. C. Mundinano *et al.*, More than blindsight: Case report of a child with extraordinary visual capacity following perinatal bilateral occipital lobe injury. *Neuropsychologia* **128**, 178–186 (2019).
44. J. M. Provis, A. M. Dubis, T. Maddess, J. Carroll, Adaptation of the central retina for high acuity vision: Cones, the fovea and the avascular zone. *Prog. Retin. Eye Res.* **35**, 63–81 (2013).
45. P. Azzopardi, K. E. Jones, A. Cowey, Uneven mapping of magnocellular and parvocellular projections from the lateral geniculate nucleus to the striate cortex in the macaque monkey. *Vision Res.* **39**, 2179–2189 (1999).
46. S. Srinivasan, C. N. Carlo, C. F. Stevens, Predicting visual acuity from the structure of visual cortex. *Proc. Natl. Acad. Sci. U.S.A.* **112**, 7815–7820 (2015).
47. G. H. Jacobs, Primate color vision: A comparative perspective. *Vis. Neurosci.* **25**, 619–633 (2008).
48. D. J. Kravitz, K. S. Saleem, C. I. Baker, L. G. Ungerleider, M. Mishkin, The ventral visual pathway: An expanded neural framework for the processing of object quality. *Trends Cogn. Sci.* **17**, 26–49 (2013).
49. N. H. Yabuta, A. Sawatari, E. M. Callaway, Two functional channels from primary visual cortex to dorsal visual cortical areas. *Science* **292**, 297–300 (2001).
50. R. Klink, A. Alonso, Ionic mechanisms for the subthreshold oscillations and differential electroresponsiveness of medial entorhinal cortex layer II neurons. *J. Neurophysiol.* **70**, 144–157 (1993).
51. T. A. Chaplin, H.-H. Yu, M. G. P. Rosa, Representation of the visual field in the primary visual area of the marmoset monkey: Magnification factors, point-image size, and proportionality to retinal ganglion cell density. *J. Comp. Neurol.* **521**, 1001–1019 (2013).
52. H.-H. Yu *et al.*, Spatial and temporal frequency tuning in striate cortex: Functional uniformity and specializations related to receptive field eccentricity. *Eur. J. Neurosci.* **31**, 1043–1062 (2010).
53. C. S. Furmanski, S. A. Engel, An oblique effect in human primary visual cortex. *Nat. Neurosci.* **3**, 535–536 (2000).
54. X. Xu, C. E. Collins, I. Khaytin, J. H. Kaas, V. A. Casagrande, Unequal representation of cardinal vs. oblique orientations in the middle temporal visual area. *Proc. Natl. Acad. Sci. U.S.A.* **103**, 17490–17495 (2006).
55. G. N. Elston, M. G. Rosa, The occipitoparietal pathway of the macaque monkey: Comparison of pyramidal cell morphology in layer III of functionally related cortical visual areas. *Cereb. Cortex* **7**, 432–452 (1997).
56. J. Tigges *et al.*, Areal and laminar distribution of neurons interconnecting the central visual cortical areas 17, 18, 19, and MT in squirrel monkey (Saimiri). *J. Comp. Neurol.* **202**, 539–560 (1981).
57. S. Shipp, S. Zeki, The organization of connections between areas V5 and V1 in macaque monkey visual cortex. *Eur. J. Neurosci.* **1**, 309–332 (1989).
58. M. A. Dyer *et al.*, Developmental sources of conservation and variation in the evolution of the primate eye. *Proc. Natl. Acad. Sci. U.S.A.* **106**, 8963–8968 (2009).
59. J. F. Mitchell, D. A. Leopold, The marmoset monkey as a model for visual neuroscience. *Neurosci. Res.* **93**, 20–46 (2015).